

Thermal Expansion in Ocean and Coupled General Circulation Models

D. R. JACKETT AND T. J. MCDUGALL

Antarctic CRC, CSIRO Division of Marine Research, Hobart, Tasmania, Australia

M. H. ENGLAND

Centre for Environmental Modelling and Prediction, School of Mathematics, University of New South Wales, Sydney, New South Wales, Australia

A. C. HIRST

CRC for Southern Hemisphere Meteorology, CSIRO Division of Atmospheric Research, Aspendale, Victoria, Australia

(Manuscript received 28 September 1998, in final form 11 June 1999)

ABSTRACT

More than half of the predicted rise in future sea level caused by the enhanced greenhouse effect is currently thought to be due to the thermal expansion of the oceans. Here methods for quantifying this thermal expansion component of sea level rise in ocean general circulation models (GCMs) are developed. A simple linear model of ocean heat uptake allows one to find an expression for the future global trend of sea level rise as a function of globally averaged sea surface temperature. The authors also present a robust procedure for obtaining spatial maps of sea level rise in three-dimensional ocean models. The authors then apply these techniques to the ocean components of three runs of the Commonwealth Scientific and Industrial Research Organisation fully coupled GCM. Two of these experiments have been performed with a recent parameterization of oceanic mesoscale eddies. It is shown that this eddy parameterization significantly lowers ocean heat uptake and future sea level rise in ocean GCMs. For the models running with the new eddy parameterization, the simple linear heat uptake model underestimates the sea level rise found in fully coupled GCMs by approximately 10%.

1. Introduction

Sea level rise is quantitatively captured by two key pieces of information: a trend line of the expected global mean sea level rise over the next 100 or so years and, at some future point in time, a global map of sea level rise variations about the mean value found at that time. The global trend can be obtained from fully coupled general circulation models (GCMs) and from simpler models of the climate system that mimic the behavior of the fully coupled GCMs, but the global sea level rise map must rely on the complexity of detail that can only be found in the fully coupled GCMs.

Here we will be concerned with both aspects of sea level rise. For the global trend, we analyze the output of an ocean-only GCM running with today's climate, and we develop a simple linear model for the subduction of heat into the interior ocean. This results in an ex-

pression for the global thermal expansion of the ocean as being a simple convolution with the global sea surface temperature (SST) time series. We then compare sea level as estimated with this linear model to the global trend in sea level that is found in three separate experiments from the Commonwealth Scientific and Industrial Research Organisation (CSIRO) fully coupled GCM (Gordon and O'Farrell 1997; Hirst et al. 2000). For the spatial map part of sea level rise, we develop an inverse method that can be used on the output from these same coupled GCM experiments to produce global maps of sea level rise.

At this stage there is little alternative to what is presently being used by the Intergovernmental Panel on Climate Change (IPCC) for estimating the global trend in future sea level under different forcings of greenhouse gases. IPCC (1990, 1992, 1996) base their sea level trend estimates on an upwelling diffusion–energy balance climate model, a model developed over the last decade by Wigley and Raper (1987, 1992, 1993). This relatively simple climate model has been tuned from the fully coupled GCMs of Cubasch et al. (1992), Manabe and Stouffer (1994), and Murphy (1995). This is achieved by selecting values for parameters such as the

Corresponding author address: Dr. D. R. Jackett, Antarctic CRC, CSIRO Division of Marine Research, GPO Box 1538, Hobart, TAS 7001, Australia.
E-mail: jackett@marine.csiro.au

climate sensitivity, the ocean upwelling rate, and the ocean vertical diffusion coefficient so that the results of the simple climate model fit the fully coupled GCMs in some sense. A problem with the coupled GCMs is still that their computational cost is so high that the simpler ocean model used by the IPCC is necessary for predicting the full range of future sea level rise corresponding to a realistic range of atmospheric forcing. It is known that the one-dimensional upwelling–diffusion ocean model also has major shortcomings (Wigley and Raper 1993).

To develop an alternate global trend model, we apply linear operator theory to the uptake of heat from the base of the ocean mixed layer to its interior. By considering the heat contents of the mixed layer and specified layers in the ocean interior, we are able to relate the internal temperature of the ocean to the ocean's SST. This is achieved by calculating Green's functions for the linear uptake of heat by the interior layers by differentiating the responses of an ocean GCM under Heaviside forcing of a passive tracer at the ocean's surface. Once the Green's functions are known, we use thermal expansion coefficients of the ocean's layers to arrive at an expression for the thermal expansion of the ocean as a function of SST.

Throughout we will be making use of the temporal residual mean (TRM) parameterization of mesoscale eddies, which makes an impressive improvement in the currently run ocean GCMs. GCMs of the ocean exhibit some well-known deficiencies, including the deep ocean being insufficiently dense, the thermocline being too diffuse, and the surface mixed layer being too deep. Recent theoretical work (Gent et al. 1995; McDougall and McIntosh 1996) has provided a new mean velocity that can be used in these models to advect tracers (including temperature and salinity). This new velocity represents the effect of mesoscale (~ 100 km) eddies on the transport of tracers. The total mean velocity of tracers is termed the TRM velocity, and the present parameterization of this new velocity is based on the work of Gent and McWilliams (1990). There is much scope for improvements in the parameterization of the TRM velocity, but already the crude parameterization of this new velocity field has led to remarkable improvements in ocean modeling. In subsequent sections we will be making comparisons between models run both with and without this TRM parameterization.

It should be pointed out that the methods developed here and the maps of sea level rise that we find in the CSIRO coupled model are for the thermal expansion component of sea level rise only. They do not include any melting or accumulation of land-based ice or any local effects of a geological nature.

Section 2 contains descriptions of the two ocean GCMs used in this study. In section 2a we give a detailed description of the Bryan–Cox ocean GCM used to estimate the ocean's thermal expansion Green's function. Section 2b then describes the CSIRO fully coupled

GCM developed at CSIRO's Division of Atmospheric Research in Melbourne, Australia. Throughout we include a discussion of the beneficial effects that the new TRM parameterization has in the ocean GCMs. In section 3a we describe how linear operator theory can be used to generate a simple model of global thermal expansion. This provides a method for estimating future global sea level trends under differing surface-forcing scenarios. Section 3b contains theory underlying the generation of the spatial maps of sea level rise in coupled GCM output. Next, section 4a presents the Green's functions for two ocean models (one running with and the other without the TRM parameterization) and compares estimates of sea level rise from these Green's functions with those found in CSIRO's fully coupled GCM. Section 4b provides spatial maps and a discussion of regional sea level rise in CSIRO's fully coupled GCMs, while section 5 concludes the paper.

2. The ocean general circulation models

a. The ocean-only GCM

The ocean model used for estimating global thermal expansion of the oceans is the modular ocean model version of the Bryan–Cox ocean general circulation model developed at the Geophysical Fluid Dynamics Laboratory (GFDL) (Bryan 1969; Cox 1984; Pacanowski et al. 1991). The basic model configuration has been described in England et al. (1994) and England and Hirst (1997), so only a summary is given here. The model geometry matches that used extensively within several recent coupled ocean–atmosphere model studies at the GFDL (e.g., Manabe et al. 1991, 1992; Stouffer et al. 1989). The model domain consists of a global coverage of the World Ocean extending from the Antarctic continent to the North Pole. The model bathymetry represents a smoothed version of the real World Ocean bottom topography. The model grid spacing is approximately 4.5° lat \times 3.75° long with 12 or 21 (see later) unequally spaced vertical levels.

The ocean model is forced at the sea surface by seasonally varying climatological boundary conditions of temperature, salinity, and wind stress. The atmosphere-to-ocean momentum flux is determined from the wind stress climatology of Hellerman and Rosenstein (1983) interpolated spatially onto the model grid and temporally at each time step. Temperature (T) and salinity (S) are damped toward the climatological values of Levitus (1982) with uniform restoring timescales of 30 days for T and 50 days for S . In both experiments considered, the ocean model is integrated with a fixed time step for T and S of one day at all depths. The integrations continue until the equilibrium criterion of England (1993) is met, which in each case requires 3000–4000 model yr.

The two experiments considered each feature a parameterization for the effect of mesoscale eddies. In one experiment, “horizontal background” (HB), the widely

used scheme of Cox (1987) is adopted to include the effect of tracer diffusion along isopycnal surfaces. We call this experiment HB because a horizontal background diffusivity must be used in order that the model remains stable. This scheme has been shown to have only a minor effect on the deep density field compared with standard Cartesian mixing models (England 1993; Hirst and Cai 1994). However, the diffusion along isopycnal surfaces creates an additional pathway for penetration of surface water into the ocean interior. Specifically, the HB experiment differs from a Cartesian mixing model (like that of England et al. 1994) only in that an additional mixing of tracers is included along the isopycnal surfaces (after Redi 1982; Cox 1987), and the horizontal diffusivity is a constant value of $A_{\text{HH}} = 0.75 \times 10^7 \text{ cm}^2 \text{ s}^{-1}$. We have chosen to follow the choice of isopycnal and horizontal diffusivity exactly as in Manabe et al. (1991, 1992).

The other experiment, labeled TRM, features the scheme of Gent and McWilliams (1990) and Gent et al. (1995) for representing the adiabatic transport effects of baroclinic eddies. This parameterization of Gent et al. (1995) is a scheme for implementing the TRM circulation in a z -coordinate model (McDougall and McIntosh 1996). The results of Danabasoglu et al. (1994), England (1995), Danabasoglu and McWilliams (1995), Hirst and McDougall (1996, 1998), and England and Hirst (1997) demonstrate that the use of this scheme results in marked increases in the deep water density and an associated reduction in convection. These studies indicate improvements in the steady-state simulation of deep temperature and salinity, and the sensitivity of transient ventilation rates to the scheme has been explored using chlorofluorocarbons (England 1995; Robitaille and Weaver 1995; England and Hirst 1997) and bomb-produced radiocarbon (Duffy et al. 1995).

Specifically, the TRM experiment differs from the HB case in that (i) a parameterization is included for the effect of eddy-induced transport as per Gent et al. (1995), (ii) the horizontal diffusivity is set to zero, and (iii) the number of model levels is increased to 21. The implementation of the Gent et al. (1995) parameterization is as detailed in Hirst and McDougall (1996). The TRM diffusivity, which determines the strength of the eddy-induced transports, is set at $1.0 \times 10^7 \text{ cm}^2 \text{ s}^{-1}$. A highly desirable feature of the Gent et al. (1995) parameterization is that it allows the model to be run with small or zero horizontal diffusivity. There is little physical justification for inclusion of horizontal diffusivity (e.g., McDougall and Church 1986), and it is retained in the other experiments solely to ensure numerical stability. It has been shown to significantly degrade model solutions—for example, by causing an unrealistically large diapycnal flux of buoyancy and by inducing large diapycnal volume transports (e.g., Veronis 1975; Böning et al. 1995; Hirst et al. 1996a).

For numerical reasons, the incorporation of TRM into ocean GCMs requires somewhat higher vertical reso-

lution than that typically used in non-TRM models. For an ocean of depth around 5000 m, about 20 levels are required when adopting TRM, compared to order 10 in non-TRM cases. As such, we construct vertical levels in our TRM runs that preserve the basic model geometry used in HB while enhancing the vertical resolution in TRM. This is achieved by splitting the deeper HB levels into two TRM levels. Because ocean ventilation and overturn is little changed in HB when resolution is increased in this manner [see appendix in England and Holloway (1998)], it was not necessary for us to rerun the HB experiments at the higher TRM vertical resolution. In particular, differences between the HB and TRM cases are almost exclusively due to differences in the lateral mixing parameterizations.

Figure 1 shows the maximum surface layer convection depth in the two experiments over the World Ocean. The maps are derived from determination of the depth attained by convective adjustment from the surface at each time step during an annual cycle of the equilibrated model runs. Included in the analysis are those regions where the slope of the isopycnal surfaces exceeds 1 part in 100 (corresponding to the maximum slope set for isopycnal diffusion), which generates vertical diffusion terms that partly mimic and replace explicit convective mixing (Hirst and Cai 1994). The HB case shows extensive deep convection in the Southern Ocean. The widespread deep convection between 55° and 70°S conflicts with observations, which suggest that this band is mostly characterized by upwelling of old circumpolar deep water and shallow surface mixed layers (e.g., Olbers et al. 1992). In contrast to HB, convection in the TRM case is largely limited to the Antarctic shelf and to north of the polar frontal zone (both thought to be regions of convective mixed-layer formation; e.g., McCartney 1977; Killworth 1983).

To diagnose the rate of surface water overturn, we take the equilibrated ocean circulation model (typically derived from a 3000–4000-yr integration) and restart the integration with an additional tracer (D) initially at zero concentration everywhere. The model is then run with the surface boundary condition $D(x, y) = 1$ unit m^{-3} for several hundred years. The concentration of tracer D is governed by the standard tracer conservation equations used for T – S .

Water in direct contact with the surface (i.e., the uppermost model level) has a dye concentration D of 1 unit m^{-3} throughout the integration, whereas the interior grid boxes are gradually filled with the surface dye at a rate determined by the ventilation timescales of the model. Water in convectively active regions will be rapidly flushed by the idealized surface dye, whereas water in the deep North Pacific might wait hundreds of years until the first significant levels of surface dye contaminate the region. The transient response of the model to the injection of dye will track the gradual renewal or flushing of the ocean system by water originating from the sea surface.

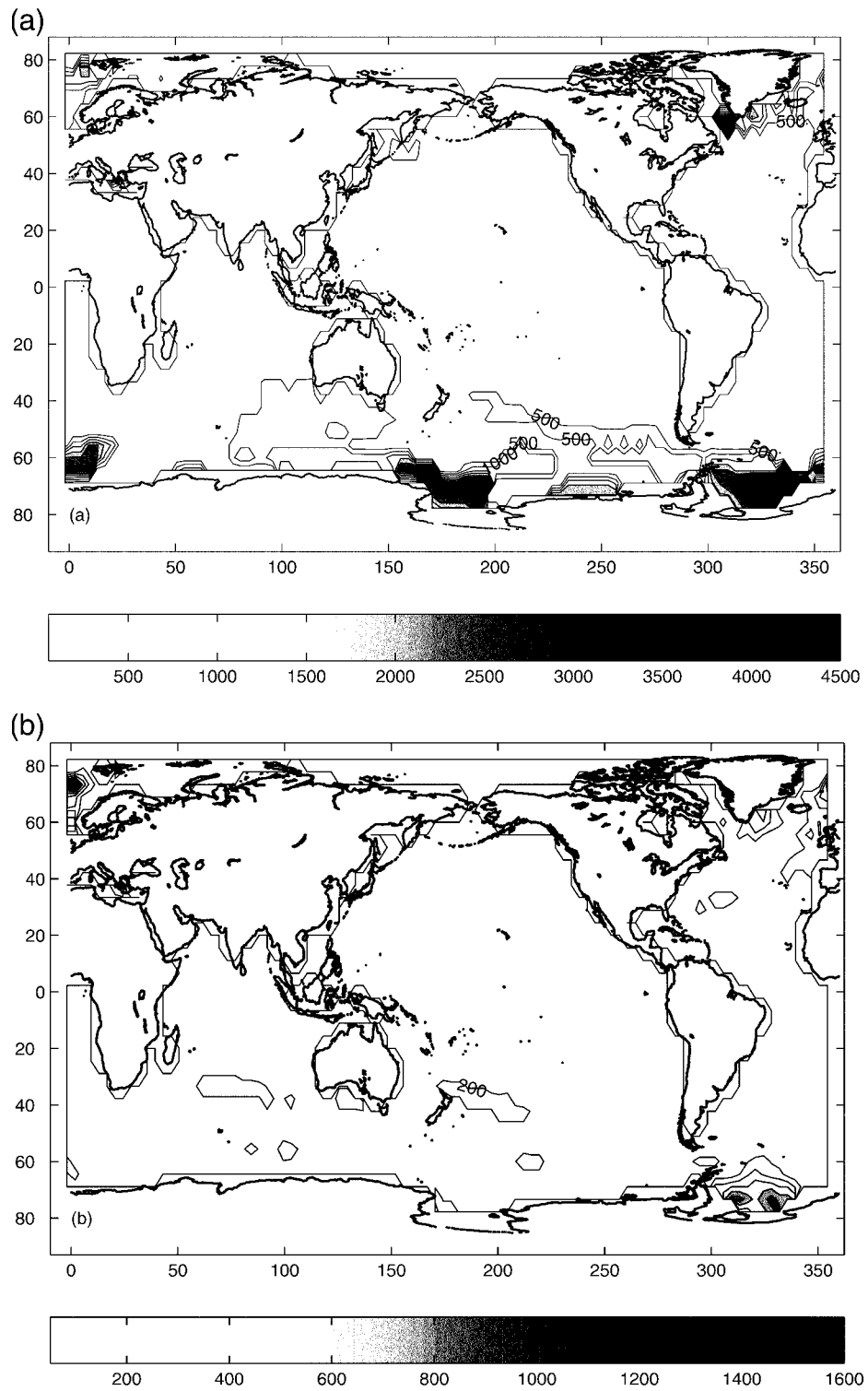


FIG. 1. Maximum depth of surface level convective overturning (m) during a complete annual cycle of the equilibrated ocean model experiments; (a) and (b) are for the HB and TRM ocean-only GCM experiments, respectively.

b. The CSIRO fully coupled GCM

The CSIRO coupled model is a comprehensive general circulation model that contains atmospheric, oceanic, sea ice, and biospheric submodels. The coupled model is described by Gordon and O'Farrell (1997) and Hirst et al. (2000), so only a brief summary is given here. The atmospheric component is spectral with horizontal resolution limited by a rhomboidal truncation at wavenumber 21. In the vertical, the atmospheric model is discretized on nine levels in a sigma coordinate system. The model has full diurnal and annual cycles, gravity wave drag, a mass flux scheme for convection, semi-Lagrangian water vapor transport, and a relative humidity-based cloud parameterization. The sea ice component is fully described in O'Farrell (1998). It includes cavitating fluid rheology and three-level ice thermodynamics. Advection and divergence of sea ice can result from both wind stress and transport by the ocean currents.

The ocean component is similar to that described in section 2a, with chief differences as follows. The temperature-salinity grid points are coincident with the physics grid of the atmospheric component, with spacing approximately $3.2^\circ \text{ lat} \times 5.6^\circ \text{ long}$. Correspondingly, the oceanic horizontal viscosity is $9 \times 10^9 \text{ cm}^2 \text{ s}^{-1}$, compared with a value of $2.5 \times 10^9 \text{ cm}^2 \text{ s}^{-1}$ used in the ocean-only GCM of section 2a. The vertical diffusivity (κ_v) is set as a function of local static stability after Gargett (1984). As for the ocean-only GCM, mixing of tracers is also performed along the neutral density surfaces according to Cox (1987) using an isopycnal tracer diffusivity of $1 \times 10^7 \text{ cm}^2 \text{ s}^{-1}$.

Results from two versions of the coupled model are presented here. The two versions differ only in their oceanic components, and we again refer to them as the HB and the TRM versions of the model. The HB version (Gordon and O'Farrell 1997) includes a horizontal background diffusivity (κ_H) that tapers from $1.2 \times 10^7 \text{ cm}^2 \text{ s}^{-1}$ at the surface to $0.5 \times 10^7 \text{ cm}^2 \text{ s}^{-1}$ in the deep ocean, with an e -folding decay depth of 500 m, and no eddy-induced advection. In the TRM coupled model (Hirst et al. 2000), the ocean component has zero horizontal background diffusivity and, instead, uses the TRM scheme of Gent et al. (1995). As for the ocean-only GCM, a TRM diffusivity of $1 \times 10^7 \text{ cm}^2 \text{ s}^{-1}$ is used. In the coupled model, this diffusivity is tapered over the top 270 m of the ocean to zero at the surface. Again, the two versions of the coupled model differ in the number of oceanic levels, with 12 in the standard version and 21 in the revised version. The increase in vertical resolution in the latter was implemented to ensure acceptable numerical behavior in the absence of horizontal diffusion. However, the increase in resolution is implemented in such a way as to provide as little impact as possible on the physical character of the solution (see Hirst et al. 2000). In summary, the differences between the two versions of the coupled model

TABLE 1. Integrations with the CSIRO coupled ocean-atmosphere model featured in the present study. All transient (global warming) integrations commence from the end of year 30 of the respective control integration.

Integration	Period of integration	CO ₂ scenario
HB—control	1000 yr	Constant (330 ppm)
TRM—control	1000 yr	Constant (330 ppm)
HB95	1973–2100	IS92a CO ₂ only
TRM96	1973–2100	IS92a CO ₂ only
TRM97	1880–2100	IS92a CO ₂ equivalent (CO ₂ and other trace gases)

correspond very closely to the differences between the two versions of the ocean-only model.

Table 1 summarizes the five coupled model integrations examined here. Control (constant CO₂) integrations are performed for both versions of the coupled model, following identical experimental procedures (Gordon and O'Farrell 1997; Hirst et al. 2000). The atmospheric and sea ice components were spun up together using climatological SST. Both versions of the ocean component were spun up in several stages totaling several thousand years of integration, using a surface restoration to climatological SST and surface salinity. Surface fluxes from the final 10 yr of the atmosphere-sea ice integration and from the final 100 yr of the two ocean integrations were saved and averaged to obtain monthly values, from which flux adjustments were calculated (see Gordon and O'Farrell 1997, their appendix). The control integrations were initialized using the final state of the atmosphere and of the respective ocean from the above spinup integrations. These integrations feature a constant atmospheric CO₂ level of 330 ppm and are continued for 1000 yr. The two control simulations were compared in Hirst et al. (2000), where it was shown that differences in stratification and convection similar to those evident between the HB and the TRM ocean-only models in section 2a are maintained for the duration of the control integrations.

Results from three transient (increasing CO₂) integrations are presented here. The first two, referred to as HB95 and TRM96 to indicate coupled model version and year of model run, both feature a prescribed atmospheric CO₂ concentration (which follows the lower curve in Fig. 10a). This CO₂ scenario is the IS92a scenario for atmospheric CO₂ alone from 1973 to 2100 (see IPCC 1992), without consideration of the radiative forcing effects of other trace gases or aerosols. The HB95 and TRM96 transient responses were compared in Hirst et al. (1996b), where it was shown that the increase in depth-integrated heat content was considerably greater in HB95 than in TRM96 in the Southern Ocean but was elsewhere similar in the zonal mean for the two integrations.

The third transient integration, referred to here as TRM97, is performed only with the TRM coupled model version and features an atmospheric CO₂ concentra-

tion (following the upper curve in Fig. 10a). This scenario is computed so as to effect the changes in radiative forcing resulting from changes in concentration of CO₂ and other trace gases, but not aerosols, according to Shine et al. (1990) and Kattenberg et al. (1996) over the period 1880–1990, then according to the IS92a scenario (Kattenberg et al. 1996) over the period 1990–2100. The early (1880) commencement avoids potential cold start errors resulting from the recent (1973) initiation of the two previous runs.

The TRM97 solution is discussed in Hirst (1999). It displays a rate of warming to the present in the Southern Hemisphere that is broadly in accord with that observed (though observational data are very poor), but a rate in the Northern Hemisphere roughly double that observed. A factor contributing to this discrepancy may be the neglect of aerosol radiative effects, which have been shown to reduce the rate of warming primarily in the Northern Hemisphere (Mitchell and Johns 1997). These effects were deliberately ignored in the forcing of TRM97, mainly because of the very large uncertainty of the size of their contribution. However, the thermal expansion component of sea level rise is a global phenomenon, and we will attempt to take some account of the aerosol effect in the presentation of results in section 4b.

3. Methodology

a. The trend model: A density-layered model of global thermal expansion

Linear operator theory provides a general mathematical setting for the trend model. Under the assumption that a response function $\phi_f(t)$ has some linear relationship with a forcing function $f(t)$ (be it via a linear differential or integral operator, or some other more complicated linear operator), then there is a Green's function $g(t)$ for which

$$\phi_f(t) = \int_0^t g(t-u)f(u) du. \quad (1)$$

This result is well known in many different disciplines of science, Green's functions also being known as (impulse) response functions, influence functions, and source functions (see, e.g., Greenberg 1971; or Butkovskiy 1982).

It follows immediately from (1) that the Green's function $g(t)$ completely determines the response of a linear system. It is also well known that the Green's function can be calculated by simply differentiating the response function $\phi_f(t)$ in (1) when the forcing function $f(t)$ is the unit Heaviside step function $\chi(t)$,

$$g(t) = \frac{\partial \phi_\chi}{\partial t}. \quad (2)$$

We use this property (2) for estimating a Green's func-

tion for the heat uptake of the internal ocean. We do this, however, using a layered model of the ocean.

Church et al. (1991) evaluated the thermal expansion component of sea level rise using a density-layered model of the ocean that was driven by changes in sea surface temperature. Their model domain is shown in Fig. 2 where we have a global ocean with a surface mixed layer lying above seven equal volume layers in the main thermocline and a larger deeper layer underneath. Heat is transferred from the surface mixed layer into the underlying eight density layers by the process of subduction along the density layers.

The layered concept in oceanography is appealing because the diffusivity with which properties are mixed across density surfaces is known to be a factor between 10⁶ and 10⁸ smaller than the diffusivity with which properties are mixed along density surfaces. This means the rate at which tracers (including a temperature perturbation) are absorbed into the ocean is governed by the rate of the lateral advection and mixing processes that happen along density surfaces. The use of a passive tracer to characterize the way in which the ocean takes up heat has been justified by the oceanic subduction arguments of Church et al. (1991) and Bindoff and McDougall (1994). They have shown that even though the density of an individual fluid parcel changes upon warming, when the parcel is subducted into the ocean interior it still contributes to sea level rise, despite the fact that its density has changed so that it may, in fact, belong in a different one of our eight layers.

The incorporation of properties into the ocean interior by subduction relies, in turn, on a host of other processes occurring in or near the surface mixed layer, including Ekman pumping, Ekman transport, turbulent mixing, and convective overturning. Our Green's function approach to characterizing a layer's tracer burden incorporates all these detailed processes to the extent that they are well represented in the GCMs. Once a fluid parcel leaves the ocean mixed layer, our physical picture is of adiabatic motion along isopycnals, but the Green's function approach is not constrained in this way. Rather, the Green's functions will include the effects of any diapycnal mixing of our tracer, whether this diapycnal mixing is by an explicit diapycnal diffusivity or is due to the horizontal diffusion across steeply sloping isopycnals (in the HB case).

The response of each layer to warming at the sea surface is thus determined from studying the behavior of a passive tracer in a global ocean model (see section 2a for a complete description of this ocean model). The global model is integrated to a steady state, and then the passive tracer is suddenly imposed at the sea surface; that is, the tracer value is instantaneously changed from 0 to 1. The tracer is then advected and diffused in the ocean model in the same manner as salt and temperature. This has been done both in a model that includes the new TRM advection scheme of Gent and McWilliams (1990) and in one that does not include this scheme (the

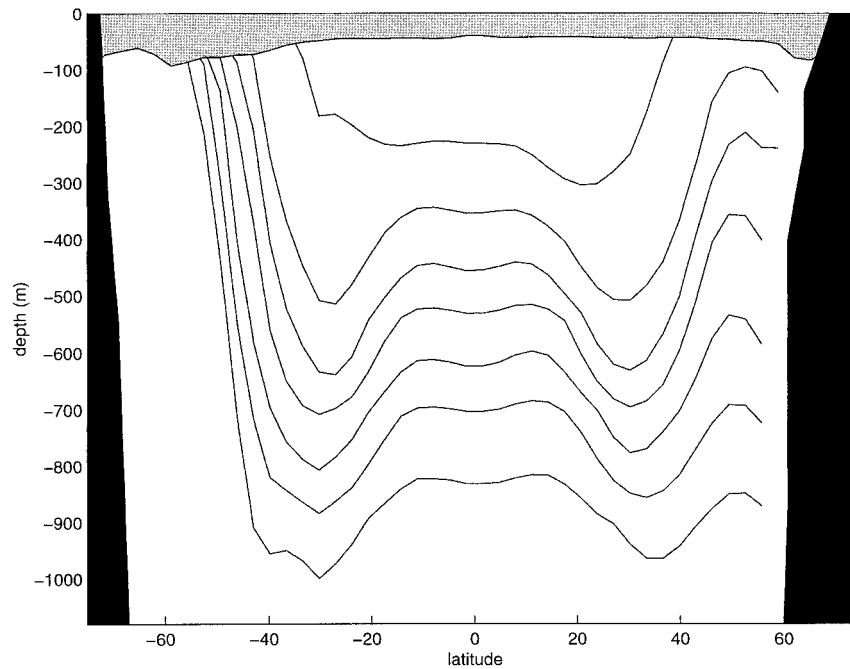


FIG. 2. Layered model of the ocean over the top 1000 m of depth showing the mixed layer and eight density layers, as found in Church et al. (1991).

HB model). Throughout, we keep track of the tracer value in the three-dimensional computational domain, allowing us to make the following calculations.

We concentrate on just one layer k and let the total volume of this layer be V_k . Consider the burden of passive tracer $B_k(t)$ in layer k at time t , that is, the volume integral of passive tracer integrated over layer k at time t . It is clear that the volume-averaged concentration of passive tracer in the interior of layer k , $c_k(t)$, is given by

$$c_k(t) = \frac{B_k(t) - B_{k0}}{V_k - B_{k0}}, \quad (3)$$

where B_{k0} is the burden of passive tracer that instantly appears in the mixed part of layer k . Since the tracer value imposed at the sea surface is unity, B_{k0} is the mixed-layer volume of layer k . Defining $b_k(t) = B_k(t)/V_k$ as the volume-averaged passive tracer value for layer k , the internal concentration $c_k(t)$ can be written alternately as

$$c_k(t) = \frac{b_k(t) - b_{k0}}{1 - b_{k0}}, \quad (4)$$

where $b_{k0} = B_{k0}/V_k$ is the mixed-layer volume fraction of layer k .

Now the average interior tracer concentration for layer k , $c_k(t)$, is the response to Heaviside forcing of the mixed-layer tracer concentration. Assuming a linear model as in (1), it follows that $c_k(t)$ can be written as the integral of the Green's function $g_k(t)$ of this layer:

$$c_k(t) = \int_0^t g_k(t-u) du. \quad (5)$$

As in (2), we simply differentiate (5) to get

$$g_k(t) = \frac{dc_k(t)}{dt}. \quad (6)$$

This we estimate numerically from the ocean-only GCM data using a multipoint (moving average) finite-difference technique developed by Anderssen and deHoog (1984).

For a general forcing function of passive tracer $f(t)$, the average interior tracer value $r_k(t)$ of layer k is now given by the convolution of the layer-forcing function $w_k f(t)$ and the layer's Green's function, so that

$$r_k(t) = w_k \int_0^t g_k(t-u) f(u) du. \quad (7)$$

Here $\{w_k, k = 1, 2, \dots, 8\}$ are layer outcrop weights determined from the sea surface temperature distribution in a coupled GCM. The volume-averaged tracer value for the whole layer $\tilde{r}_k(t)$ is now the volume-weighted average of the mixed-layer tracer value $w_k f(t)$ and the interior value $r_k(t)$:

$$\tilde{r}_k(t) = b_{k0} w_k f(t) + (1 - b_{k0}) w_k \int_0^t g_k(t-u) f(u) du. \quad (8)$$

Expansion coefficients χ_k ($\text{m}^\circ\text{C}^{-1}$) can be computed

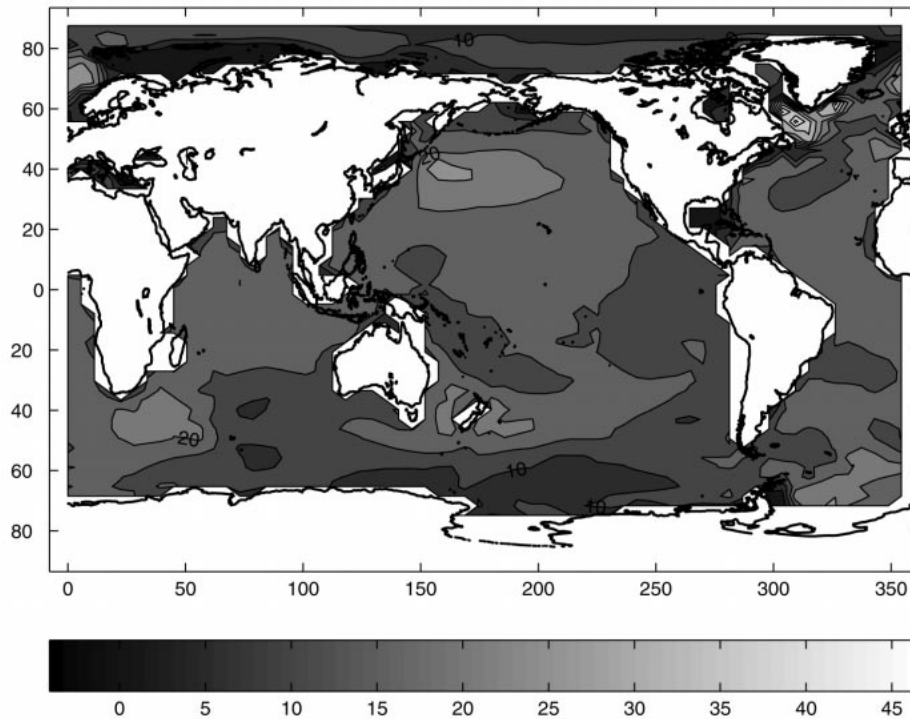


FIG. 3. Dynamic height (cm) map from the ocean floor to the sea surface of the CSIRO coupled model at the time of atmospheric CO_2 doubling.

from a coupled GCM by taking appropriate volume integrals of the thermal expansion coefficient $\alpha = -(1/\rho)\partial\rho/\partial\theta$ (ρ being the in situ density of seawater and θ being the potential temperature) between the layer interfaces. (The contribution of salinity changes to the thermal expansion of seawater was found to be less than 1.5% in CSIRO's coupled GCM and so has been ignored.) These can then be used to infer the contribution $\chi_k \tilde{f}_k(t)$ to sea level rise from layer k . The globally averaged sea level rise $h(t)$ that results from a given global forcing function $f(t)$ is found by summing these contributions $\chi_k \tilde{f}_k(t)$ over all layers k and can be written from (8) as

$$h(t) = Af(t) + \int_0^t g(t-u)f(u) du, \quad (9)$$

where

$$A = \sum_{k=1}^8 \chi_k w_k b_{k0} \quad \text{and} \quad (10)$$

$$g(t) = \sum_{k=1}^8 \chi_k w_k (1 - b_{k0}) g_k(t).$$

The constant A is an effective mixed layer depth times an appropriate thermal expansion coefficient, so that the first term in (9) is the globally averaged thermal expansion due to the temperature change of mixed layer fluid in the World Ocean. Similarly, the response func-

tion $g(t)$ is the Green's function for the contribution of the ocean interior to global thermal expansion, obtained by summing the contributions to thermal expansion over all layers of our density-layered model.

b. Spatial maps of sea level rise

Spatial maps of sea level rise can really only be made from the ocean components of fully coupled models of the earth's climate system. In this section we present a method for obtaining global maps of sea level rise from such climate models. To illustrate the method, we will produce maps for the latest run of the CSIRO coupled model, the run that commenced in 1880, capturing the full impact of greenhouse warming from early industrial times.

An obvious method for estimating sea level rise is to calculate changes in the dynamic height of the sea surface relative to the ocean floor between the transient and control runs. Figure 3 shows the result of doing this for the CSIRO coupled model at the time of CO_2 doubling (2026–2035) relative to 1880 levels. This calculation is straightforward, being just the difference in the volumes of vertical water columns due to the changing hydrographic fields.

The ocean component of the CSIRO coupled model to date is a "rigid-lid" ocean model, implying additional calculations if we are to know the pressure at the top of the ocean model (being synonymous with sea level).

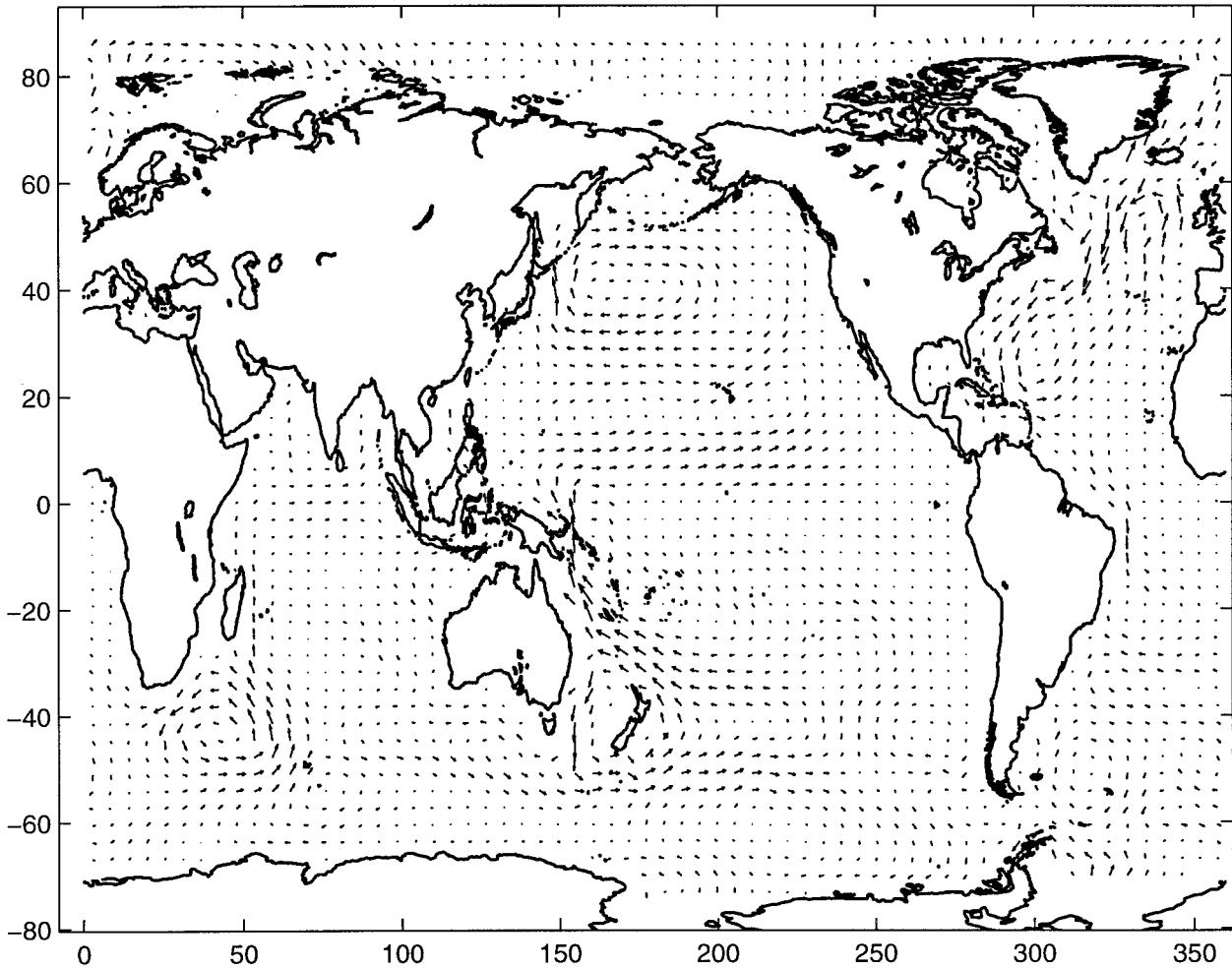


FIG. 4. Transient minus the control velocities at level 6 (185 m) of the CSIRO coupled model at the time of atmospheric CO_2 doubling.

Equivalently, we could find the pressure distribution at any level of the coupled model (and its associated sea level rise), which is possible from differences in the velocities between the control and transient runs. Figure 4 shows these differences at level 6 of the CSIRO coupled model (185 m), just below the mixed layer.

We want the spatial pattern of pressure at a fixed depth z_k in the ocean (corresponding to one of the depth levels of the CSIRO model). It is now assumed that the horizontal velocity is in geostrophic balance with the pressure field at depth z_k . For most of the ocean this is a good assumption, particularly away from continental boundaries and below the energetic near-surface flow, well below the wind-driven Ekman layer. The geostrophic balance implies that the difference between the horizontal velocities at the end of the CSIRO transient model run, and at the same time in the control run, $(\Delta u, \Delta v)$, is related to the corresponding change in pressure, Δp , by

$$\partial \Delta p / \partial x = f \rho_0 \Delta v \quad \text{and} \quad \partial \Delta p / \partial y = -f \rho_0 \Delta u. \quad (11)$$

Here f is the Coriolis parameter and ρ_0 is a reference density, taken to be 1035 kg m^{-3} . Boundary equations at continental edges are given by (11) with Δu and Δv both being set to zero. These equations can be applied at a single depth throughout the global ocean, giving an overdetermined system of equations for the pressure difference field, $\Delta p(x, y)$, at depth z_k . The area-average value for this pressure difference is set to zero. The contribution of this pressure field to sea level rise at any location then comes from the hydrostatic equation by dividing the computed pressure by $g \rho_0$, where g is the acceleration due to gravity.

The total sea level rise from thermal expansion is now obtained by adding a generalization of the single dynamic height map previously mentioned to the height field derived from the spatial pattern of pressure at depth z_k . For each level k there is a steric effect over the depth range from z_k to the sea surface, determined by evaluating the change in dynamic height between these two levels at every (x, y) location in the model. There is also

a change in volume of the fluid below z_k caused by changes in temperature and salinity in this depth range. Since we have already calculated the spatial pattern of pressure changes at z_k , the relevant contribution of the thermal expansion of the ocean below this depth is the globally averaged sea level change from this expansion. This is calculated from the same steric calculation procedure, using the changes in dynamic height at each location, but now the water column is integrated from the sea floor to z_k , and this contribution to sea level rise is averaged throughout the World Ocean.

Putting this mathematically, we know that for each level k , total thermal expansion at time t , $\mathbf{H}(t)$, is given by

$$\mathbf{H}(t) = \mathbf{H}_k^s(t) + \mathbf{H}_k^p(t) + h_k(t), \quad (12)$$

where $\mathbf{H}_k^s(t)$ is the steric effect over the depth range from z_k to the sea surface, $\mathbf{H}_k^p(t)$ is the height map derived from the spatial pattern of pressure at depth z_k , and $h_k(t)$ is the globally averaged sea level change below z_k (a scalar). Here all three maps $\mathbf{H}(t)$, $\mathbf{H}_k^s(t)$, and $\mathbf{H}_k^p(t)$ are considered as two-dimensional arrays of heights (height being 0 on land), the two dimensions being longitude and latitude.

We point out that even though we expect the final fields of sea level rise $\mathbf{H}(t)$ to be independent of the level k chosen, the two maps that go into making up sea level rise at any particular depth, namely, $\mathbf{H}_k^s(t)$ and $\mathbf{H}_k^p(t)$, can be quite different. Figures 5 and 6 clearly demonstrate this, by comparing maps made just below the surface mixed layer (185 m for Fig. 5) with maps made at the base of the main thermocline (905 m for Fig. 6). Figures 5a and 6a show the steric height maps $\mathbf{H}_k^s(t)$ from the reference depth to the ocean surface, while Figs. 5b and 6b show the height adjustments $\mathbf{H}_k^p(t)$ made from solving the geostrophic relations (11) for pressure. Figures 5c and 6c are the sum of Figs. 5a and 5b, and 6a and 6b, respectively, plus the globally averaged sea level rise $h_k(t)$ below level k , as in Eq. (12). We would expect Figs. 5c and 6c to be independent of the level k chosen for the sea level rise calculations. Figures 5c and 6c are, in fact, graphically very similar, where clearly the components making up Figs. 5c and 6c—Figs. 5a,b and 6a,b, respectively—are quite different. Maps are for the decade when equivalent CO_2 doubling occurs in the atmosphere, 2026–2035.

The method of solution we chose for (11) is the two-dimensional analog of the three-dimensional technique used for the inversion of neutral density (see Jackett and McDougall 1997). The basic idea is to treat the differential equations, when discretized on various numerical grids, as overdetermined linear systems. [For the present differential equation, no matter which grid was chosen for the global discretization of (11), the resulting system of algebraic equations was overdetermined.] Using inverse theory we can easily find the least squares solution to this problem. For an artificial velocity field obtained from differentiating a given pressure field, this inversion

technique was found to yield the exact pressure field. The technique inverts for the pressure field that satisfies Eq. (11) in a least squares sense, given the changes in the horizontal velocity components between the control and the transient runs of the CSIRO coupled model.

The geostrophic relations (11) were discretized on a variety of grids, each of these discretizations resulting in a linear system of roughly 3000 equations in 2000 unknowns. This is a computationally expensive task. Importantly though, almost identical solutions were obtained when using (12) for any level k between the bottom of the mixed layer (~ 100 m) and the bottom of the main thermocline (~ 1000 m). We did not take the solution any deeper than 1000 m due to the effect of the ocean bathymetry below this depth on the coverage of the map.

The decomposition (12) of the thermal expansion component of sea level rise into two quite distinct maps $\mathbf{H}_k^s(t)$ and $\mathbf{H}_k^p(t)$ permits a test of the accuracy of numerical schemes designed for the solution of systems of differential equations like (11). It is a simple matter to think up quite elementary numerical schemes for filling out the two-dimensional pressure field from knowing pressure at just one point in x - y space. For example, lateral integration of (11) in the x -direction followed by integration in the y -direction, with this process being repeated until the full two-dimensional pressure field has been obtained, is one such technique. Figure 7 shows the total thermal expansion from using the decomposition (12) for this simple scheme, once for level 6 (Fig. 7a) and again for level 12 (Fig. 7b). Again the maps are for the decade of equivalent CO_2 doubling of the atmosphere, 2026–2035, relative to 1880. Inspection of these maps shows regions of the globe where there are significant differences in predicted sea level rise. These differences should be compared with the negligible differences between Figs. 5c and 6c for the least squares method. This means the least squares method is consistent between levels, compared to the simpler numerical scheme, which is not. Clearly, this demonstrates the need for the extra computational effort required by the least squares solution technique.

4. Results

a. Global sea level trend

In Fig. 8 we have plotted response functions to the instantaneous forcing of $D = 1$ unit m^{-3} for all eight layers of the density-layered ocean model calculated from the ocean GCM experiment of section 2a. We have shown results for timescales of 20 and 400 yr and for the HB and TRM runs of the ocean-only GCM. It is interesting to observe from the figure that the response times for the layers increase monotonically from layers 1 to 8 in the TRM case. This accords with how one imagines subduction and mixing activity in the ocean may vary smoothly from the equator to the Poles. For

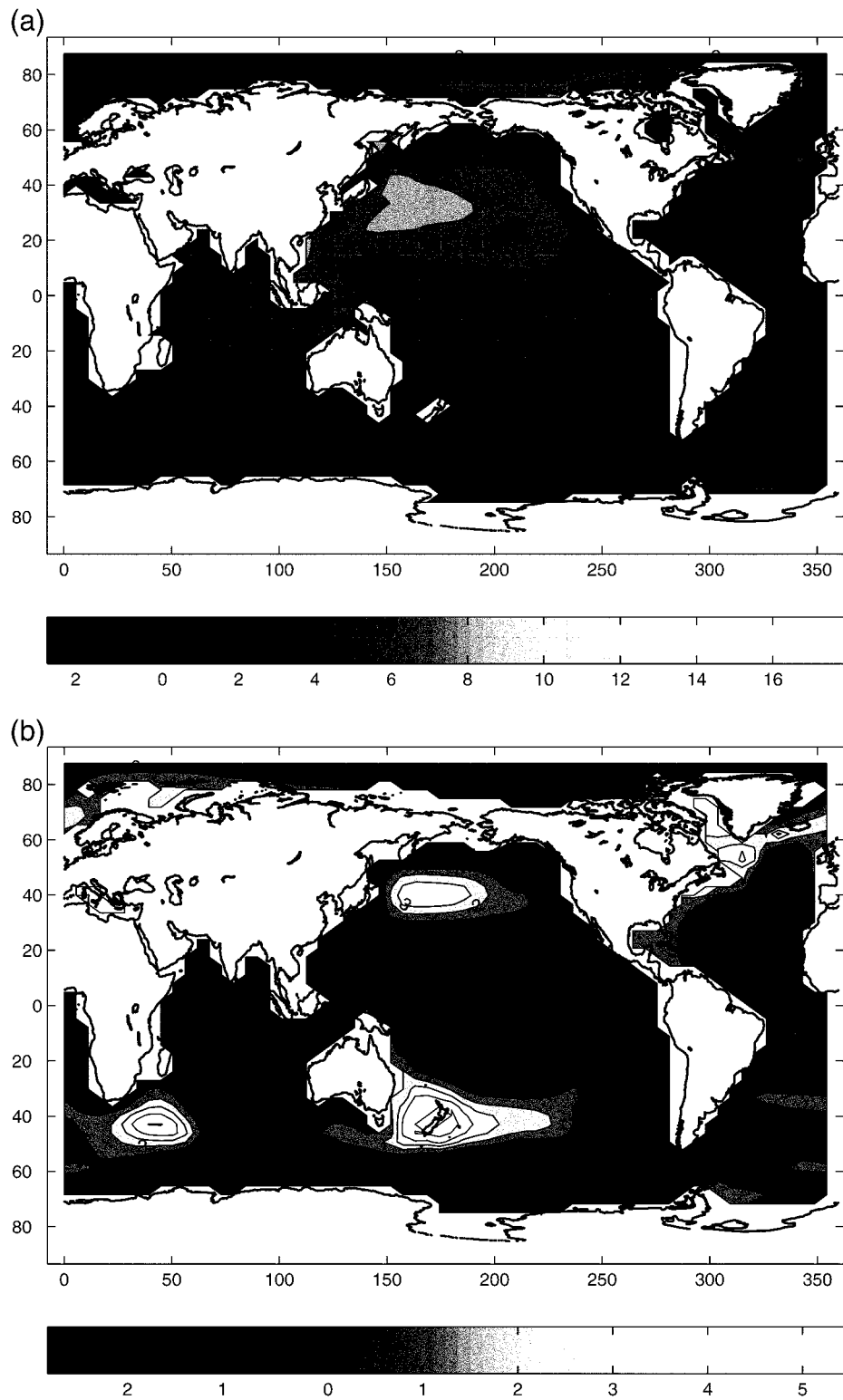


FIG. 5. (a) Steric height (cm) map from level 6 (185 m) of the CSIRO coupled model to the sea surface. (b) Height adjustment (cm) from the spatial map of pressure at level 6 (185 m) of the CSIRO coupled model.

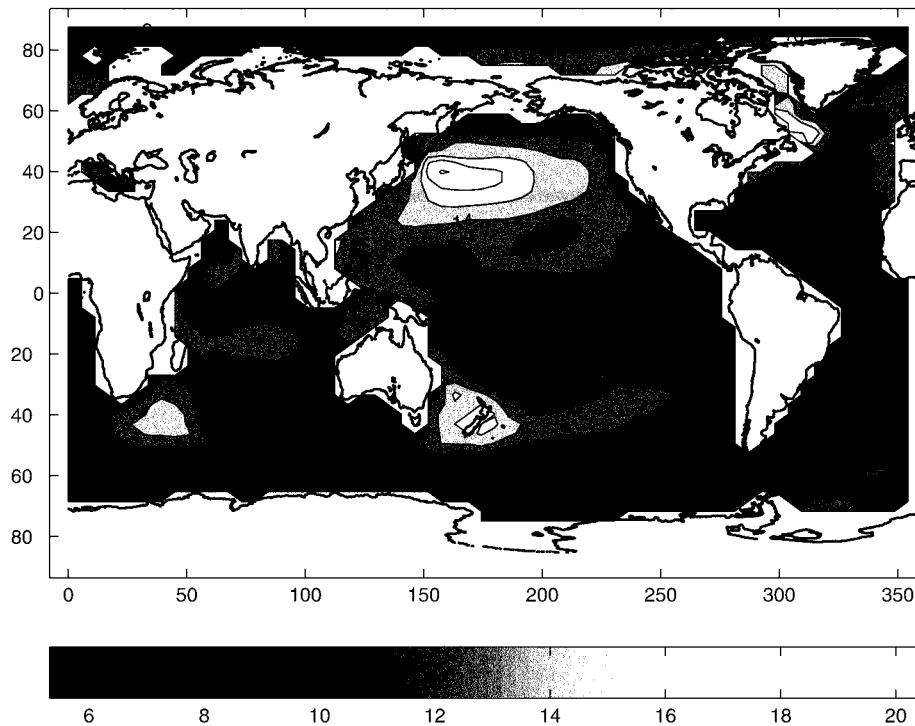


FIG. 5 (Continued) (c) The total thermal expansion component of sea level rise (cm) deduced from level 6 (185 m) of the CSIRO coupled model. The maps in this figure are for the time of CO_2 doubling in the atmosphere (relative to 1880 levels).

the HB model, the response functions for the eight layers do not vary monotonically with layer number, and one assumes that this is a reflection of the excessively deep convection that occurs in specific regions in high latitudes.

The data from the ocean-only GCM experiment of section 2a were annually averaged at 6-monthly time intervals. This eliminates the effect of the seasonal forcing in the ocean GCM experiment on the various response functions. The response of the ocean at time 0 was estimated by quadratically extrapolating the values less than a year back to the time origin. The effect of varying the extrapolation method back to the time origin was investigated and found to be insignificant.

Figure 9 shows the result of differentiating the HB and TRM response functions and adding, as in Eqs. (9) and (10), to get the overall Green's function of the ocean's sea level response to surface warming for the HB and TRM model runs of the ocean-only GCM of section 2a. The corresponding mixed-layer thermal expansion coefficients are 2.11 and $1.85 \text{ cm } ^\circ\text{C}^{-1}$ for the HB and TRM model runs, respectively. It is clear from this figure and from the size of the mixed-layer constants that sea level rise computed from the TRM Green's function and expansion coefficient will be significantly smaller than that computed from the HB model results.

The technique for taking derivatives of the response functions is based on a method found in Anderssen and deHoog (1984) that provides an asymptotically unbiased

estimate of the derivative of discrete data as weighted averages of derivatives of the data over larger and larger length scales. The length scale is at the choice of the user, the larger length scales reducing the higher-frequency oscillations in the derivative estimate of the underlying signal. We chose an uppermost length scale of 6 yr.

Figure 10 shows output from the three runs of the CSIRO coupled model as described in section 2b. Figure 10a shows atmospheric-equivalent CO_2 forcing for the three models, the atmospheric forcing for the HB and TRM models commencing in 1973 being identical with each other. In Fig. 10b we have plotted SST in the coupled GCMs as a function of time. Finally, in Fig. 10c we have shown global-average sea level rise in the coupled GCM runs (solid lines), as well as estimates of global-average sea level rise (dashed lines) from Eqs. (9) and (10), using the appropriate Green's function in Fig. 9 and the SSTs in Fig. 10b.

From Fig. 10 it is evident that there is a significant decrease in sea level rise when the TRM parameterization of eddies is included in the ocean GCMs. For the HB and TRM runs of the CSIRO fully coupled model begun in 1973 and forced with the same CO_2 increase (the light line in Fig. 10a), there is a 12% reduction in sea level rise at 2100 relative to 1990. In the case of the Green's functions estimates of sea level rise, this reduction is almost 25% at 2100 relative to 1990.

It is also clear from Fig. 10 that sea level rise esti-

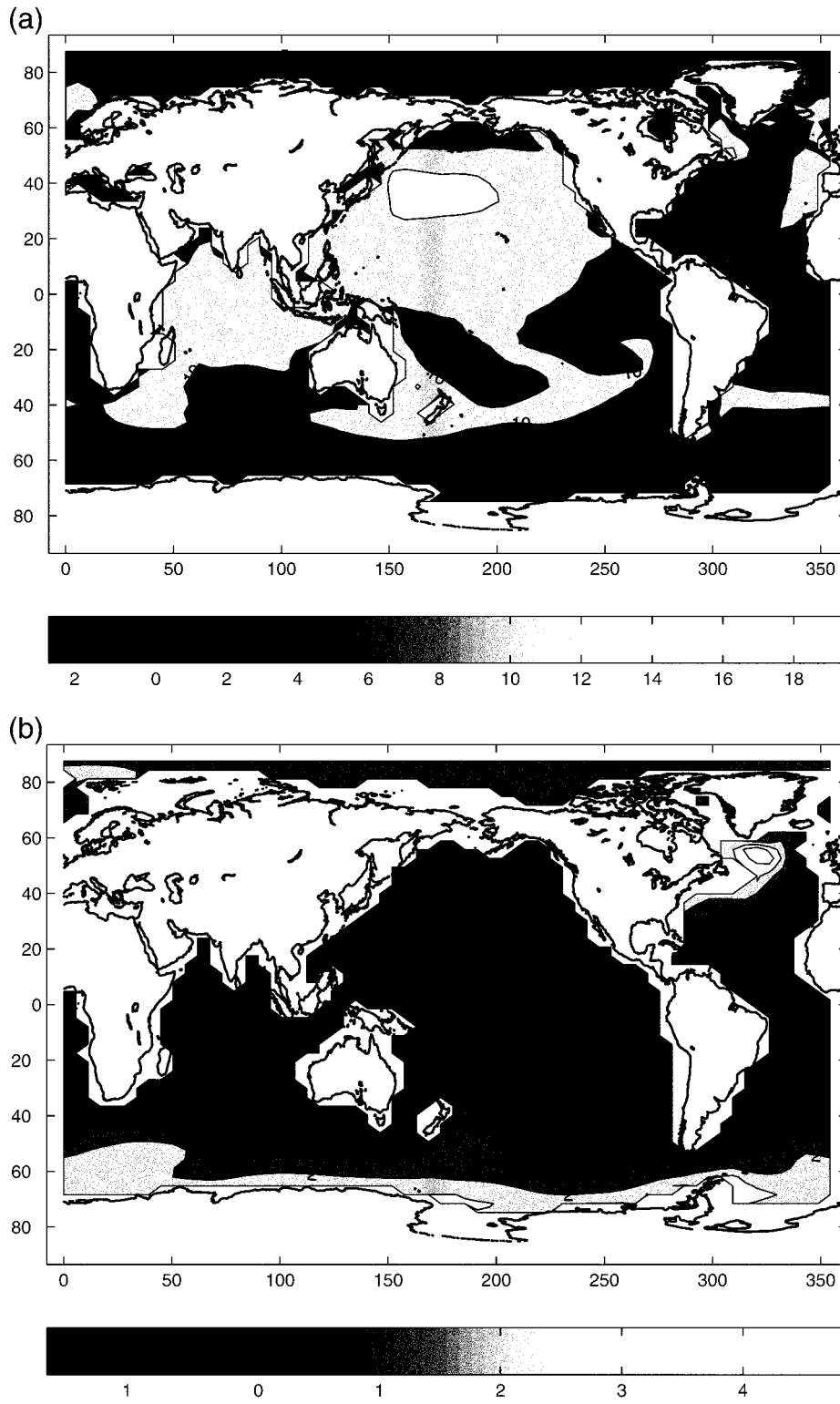


FIG. 6. (a) Steric height (cm) map from level 12 (905 m) of the CSIRO coupled model to the sea surface. (b) Height adjustment (cm) from the spatial map of pressure at level 12 (905 m) of the CSIRO coupled model.

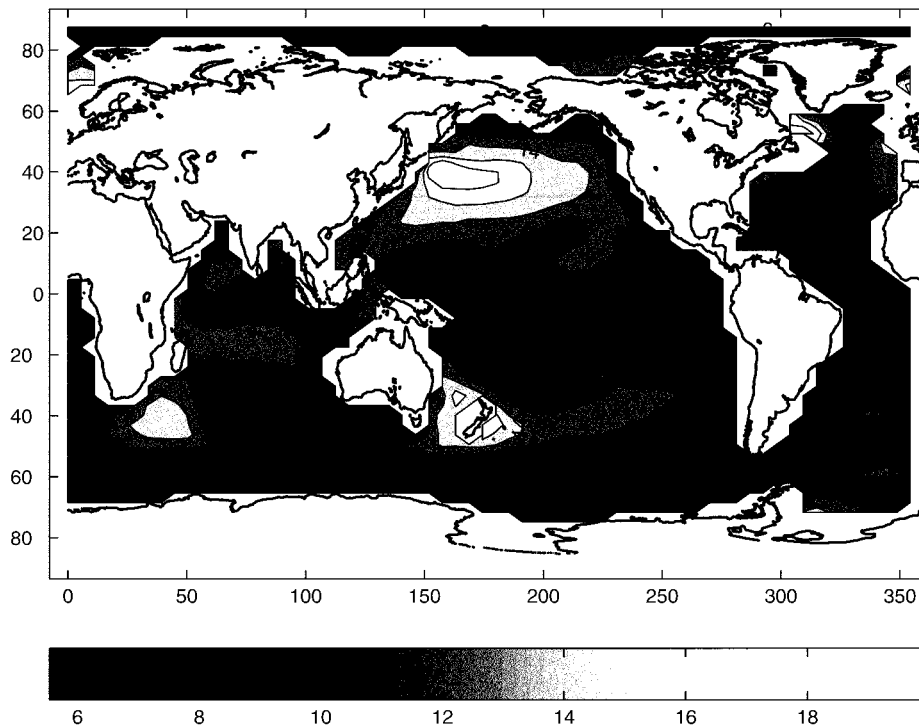


FIG. 6 (Continued) (c) The total thermal expansion component of sea level rise (cm) deduced from level 12 (905 m) of the CSIRO coupled model. The maps in this figure are for the time of CO_2 doubling in the atmosphere (relative to 1880 levels).

mated from the TRM Green's functions underestimates sea level rise in the corresponding fully coupled GCMs (9.4% for TRM96 and 12.3% for TRM97 at 2100 and 2095, respectively). In the HB model the sign of this difference is reversed, with the Green's functions estimate being 5.8% larger than the corresponding coupled GCM's estimate at 2100. There are several reasons for this difference in the sea level rise estimates. One difference between the fully coupled GCM estimates and those from the Green's functions is that those from the latter are from an ocean-only GCM running with today's climate. This means the Green's functions will not have captured any of the changing dynamics. It is well known, for example, that transient fully coupled ocean-atmosphere GCMs exhibit a slowing of the thermohaline circulation with increasing ocean temperature (see Raper et al. 1996; or Hirst 1999). In addition, the two different ocean models have different horizontal resolution, different forcing by the curl of the wind stress, and different ocean spinup techniques. The use of flux corrections in the coupled GCMs will also affect the accuracy of the predicted sea level rise estimates.

The only difference between the two TRM runs of the CSIRO fully coupled GCM is in the CO_2 forcing, as in Fig. 10a. The run begun in 1880 will clearly have a larger radiative forcing on the ocean than the run begun in 1973, both runs commencing with a CO_2 level of 330 ppm. We agree with Raper and Cubasch (1996)

that it is crucial for climate models to be compared only when their atmospheric forcings are the same. To achieve this we downscale the CO_2 forcing of the longer model run by a constant, chosen so that the total radiative forcing (see Kattenberg et al. 1996, p. 320) for both TRM runs of the CSIRO coupled model are the same over the period 1973–2100. When this is done we get sea level rise estimates of 17.9 and 20.0 cm for the two TRM runs of the CSIRO fully coupled GCM, both figures being relative to 1990 levels. The difference is due to the fact that we have not cold-start corrected (Hasselmann et al. 1993) the 17.9-cm estimate from the CSIRO model that commenced in 1973.

b. Spatial map of sea level rise

Data from the five runs of the CSIRO coupled model of section 2b were averaged into 10-yearly means, and sea level for each of the three global warming runs was computed relative to the respective control run for each 10-yr period. Figures 11–13 show global maps of sea level rise for the three global warming runs at 2091–2100 relative to 1971–1980. We have used the least squares technique of section 3b to produce these maps due to the robustness of this procedure. Also, the TRM97 response shown here has been scaled by a uniform factor of 0.74. This scaling factor represents the ratio of radiative forcing change between 1973 and 2100

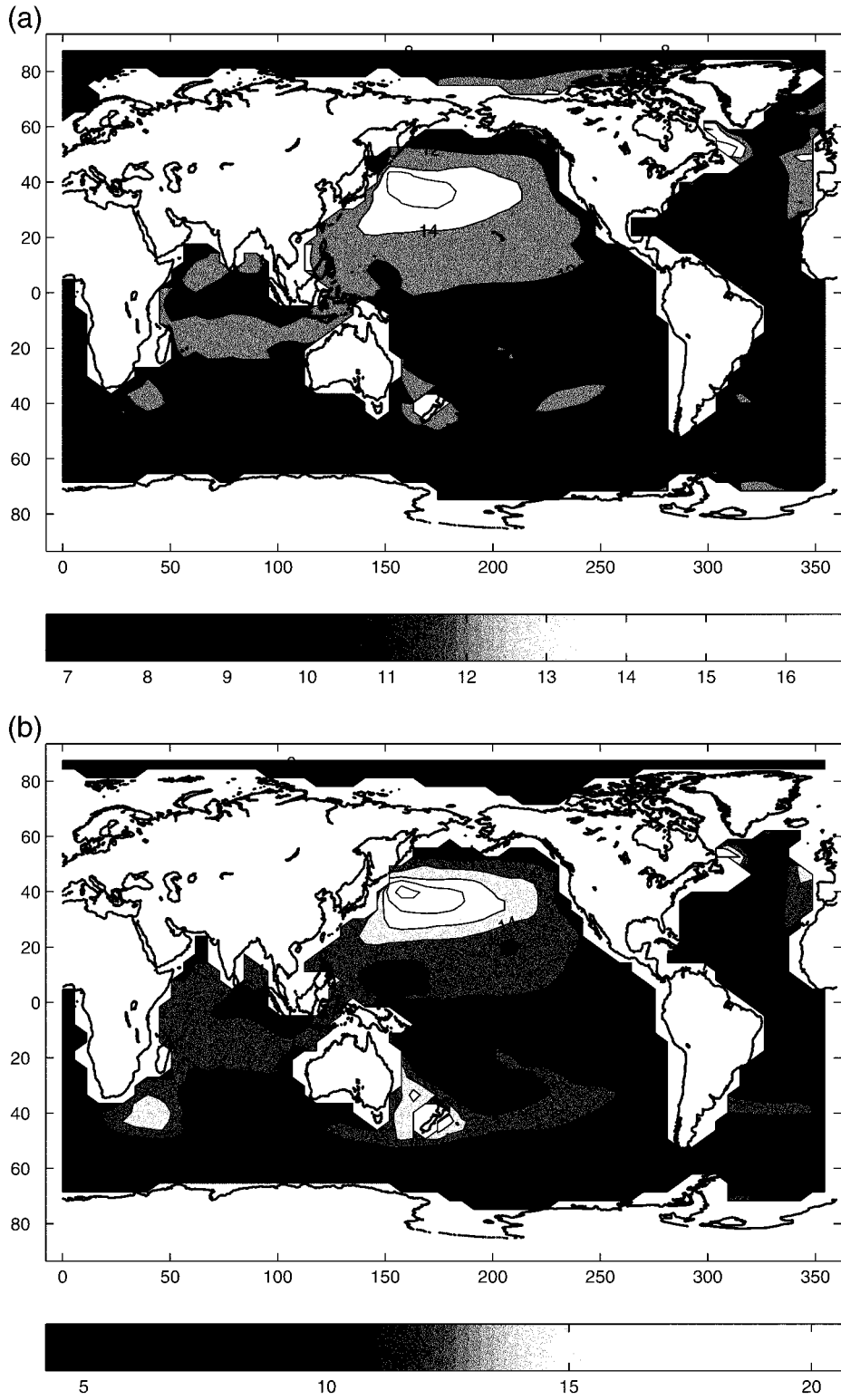


FIG. 7. (a) The total thermal expansion (cm) deduced from level 6 (185 m) of the CSIRO coupled model using a simple numerical scheme. (b) The total thermal expansion (cm) deduced from level 12 (905 m) of the CSIRO coupled model using a simple numerical scheme.

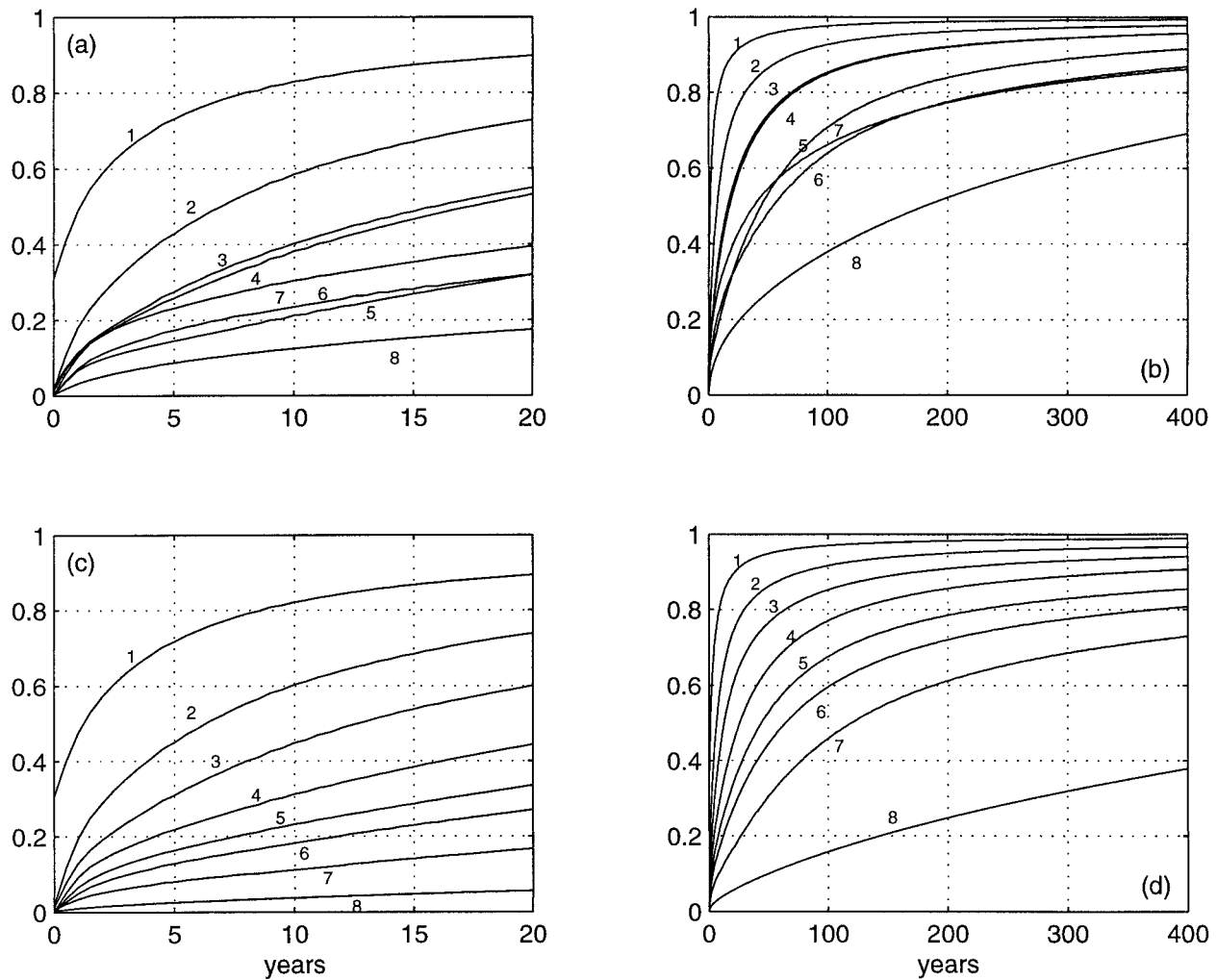


FIG. 8. The response functions $b_i(t)$ to the instantaneous forcing of $D = 1$ unit m^{-3} for each of the eight layers for both (a) and (b) the HB model and (c) and (d) the TRM model. The response functions are shown for both 20- and 400-yr timescales, and the numbered lines indicate layer numbers.

for the former two (CO_2 only) transient runs relative to the (CO_2 plus trace gases) TRM97 run and allows more direct comparison of the pattern of response. We prefer to scale the latter run's response downward, rather than vice versa, because we believe the TRM97 Northern Hemisphere warming to be excessive (Hirst 1999) as a result of neglect of the radiative effects of sulfate aerosols. Since the effect of excessive warming on sea level in one region is rapidly transmitted throughout the global ocean (on barotropic adjustment timescales), we expect the sea level rise to be generally biased upward in this run as a result. We further note that the reduction of global mean radiative forcing resulting from sulfate emission increase almost exactly offsets the change due to non- CO_2 trace gases throughout the next century, under the highest sulfate impact scenario of Kattenberg et al. (1996, their Fig. 6.19). Thus a CO_2 -only induced change in radiative forcing (as in HB95 and TRM96)

may more closely mimic the net change resulting from CO_2 plus trace gases plus aerosols than that resulting from just CO_2 plus trace gases (as in TRM97), in the global average.

There is spatial similarity between the patterns for the two TRM runs of the CSIRO coupled model (Figs. 12 and 13), but they are both very different to that for the HB95 run (Fig. 11). For example, Fig. 11 has the largest sea level rise in the Southern Ocean, whereas both Figs. 12 and 13 have the smallest sea level rise in the Southern Ocean. This is because of the different spatial penetrations of heat into the interior ocean that is caused by the inclusion of mesoscale eddies in the ocean GCMs. Notice that there is more similarity between the 1996 TRM run of the CSIRO coupled model and the maps of sea level rise in the 1997 TRM run taken at the time of CO_2 doubling relative to 1880 (i.e., Figs. 5c and 6c) than between Figs. 12 and 13. That is,

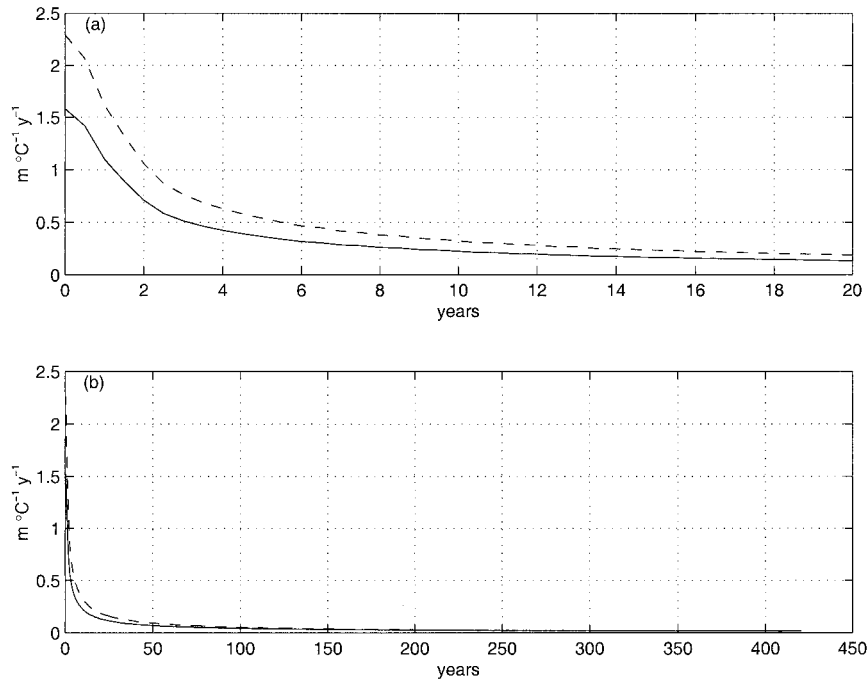


FIG. 9. Sea level rise Green's functions for the HB (dashed line) and TRM (solid line) ocean-only GCMs; (a) and (b) show the Green's functions over 20- and 400-yr timescales, respectively.

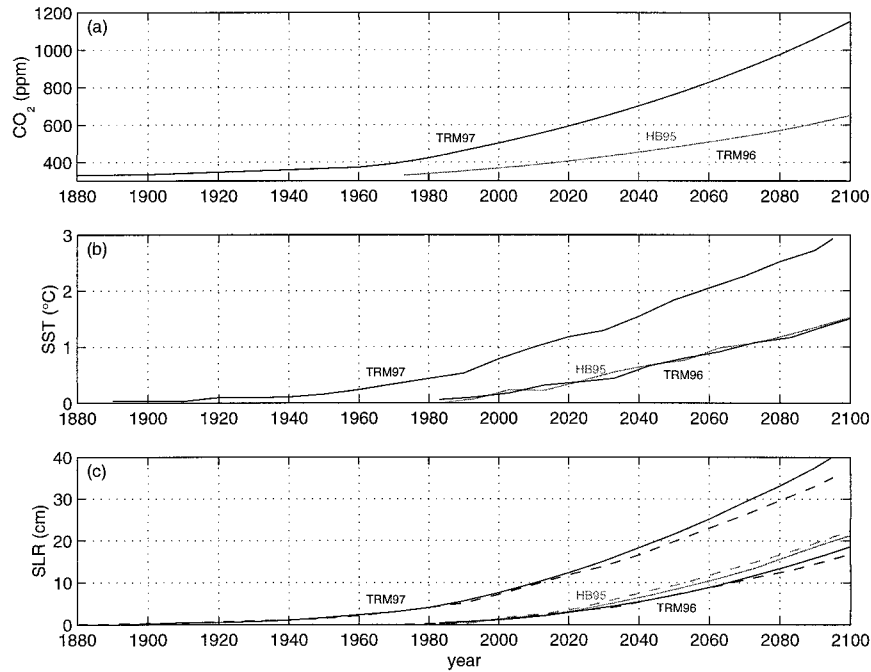


FIG. 10. Output from three runs of the CSIRO fully coupled GCM: (a) shows CO_2 levels (ppm), (b) is SST ($^{\circ}\text{C}$), while (c) shows sea level rise (cm). In each plot, the two dark full lines are the two TRM runs, while the light full line is the HB run. CO_2 forcing in (a) is identical for the HB95 and TRM96 coupled model runs. The dashed lines in (c) are computed by convolving the SSTs of (b) with the appropriate Green's function in Fig. 9, as in Eq. (9).

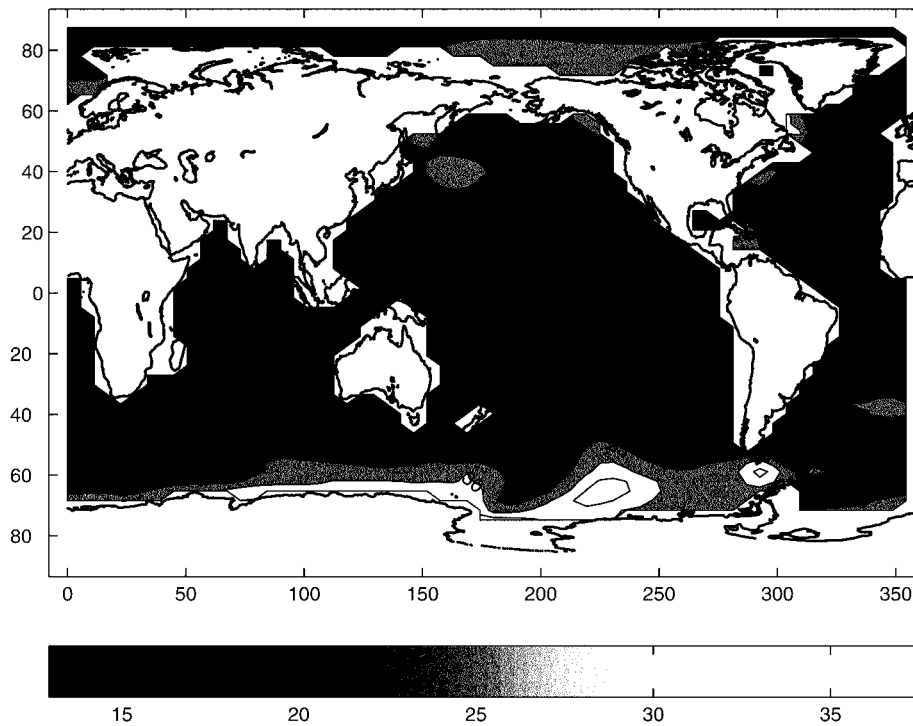


FIG. 11. The thermal expansion component of sea level rise (cm) at the end of the 1995 HB run of the CSIRO coupled model.

the two different TRM coupled model runs exhibit similar spatial maps of thermal expansion when sampled at times when the concentration of equivalent CO_2 is similar, but at the highest level of CO_2 (Fig. 13), the spatial pattern has changed. The reasons for this change in spatial pattern are unknown.

Gregory (1993) calculated a global map of sea level rise from a global coupled GCM. This map showed extreme regional variations; for example, near New Zealand there was a region that had no rise of sea level, while there were other places (such as the northwest Indian Ocean) that had a rise 50% greater than the global mean. Comparing the extremes of Gregory's Fig. 9 with those in Figs. 12 and 13 here shows that the maxima we have southeast of the African continent, adjacent to New Zealand and in the western North Pacific, do not occur in Gregory's map. The western North Atlantic high and the high sea levels in the western North Indian Ocean (in Fig. 13), as well as the low sea level north of the Ross Sea, are, however, consistent with similar patterns found in Gregory's map. The spatial patterns found in more recent maps (J. Gregory 1999, personal communication) compare much more favorably with those found in Figs. 12 and 13.

Cubasch et al. (1994) also consider the spatial pattern of sea level rise, using a free-surface ocean model. Their map (their Fig. 16a) is for the year 2035 relative to 1985, which we compare with Figs. 12 and 13. All maps show large sea level rise in the North Pacific and in a

broad region centered on New Zealand. The Cubasch map, though, has largest sea level rise in the northernmost part of the east Pacific, while we have a large rise (not the largest) in the western Pacific in Fig. 12. The Cubasch map does not have the large sea level rise we observe in the North Atlantic in both our maps, and in the Southern Hemisphere some of the local maxima (or minima) of sea level rise over large areas are inverted between the Cubasch maps and Figs. 12 and 13.

Bryan (1996) presents a global map of dynamic height from the sea surface to a depth of 1130 m and discusses it as though it is a map of sea level rise. However, we know from Figs. 3, 5c, and 6c that there are very significant contributions to sea level that are due to changes below this depth. Bryan (1996) does correct his steric height map for the ocean dynamics but shows only the North Atlantic portion of the ocean: he concentrates on the change in the thermohaline circulation under the greenhouse effect, and the structure he uncovers in the North Atlantic shows the way in which the model shuts down its production of North Atlantic deep water.

The maps of Gregory (1993) and Cubasch et al. (1994) are the only published maps that are directly comparable to the sea level rise maps shown in Figs. 12 and 13. Despite some striking similarities between these maps, there are large differences over some substantial geographical areas. More than most model features, these published maps of sea level rise from dif-

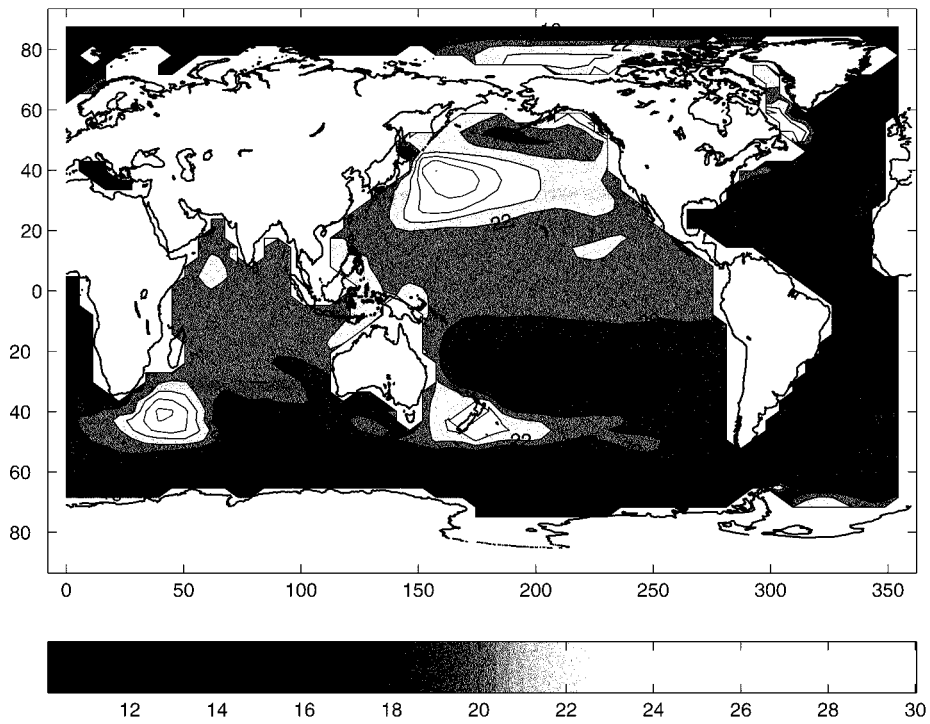


FIG. 12. The thermal expansion component of sea level rise (cm) at the end of the 1996 TRM run of the CSIRO coupled model when the equivalent CO_2 concentration was 652 ppm.

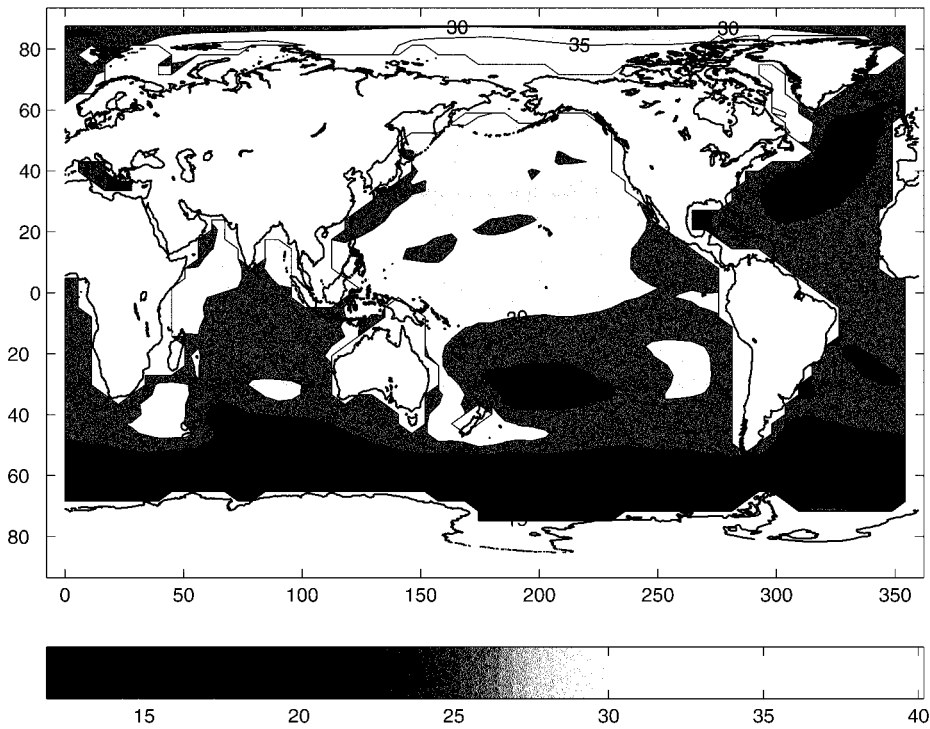


FIG. 13. The thermal expansion component of sea level rise (cm) at the end of the 1997 TRM run of the CSIRO coupled model when the equivalent CO_2 concentration was 1155 ppm.

ferent ocean models are quite different. With the inclusion of eddy parameterizations in coupled GCMs, however, the spatial variability found in the maps of sea level rise from the different research groups are becoming much more similar (J. Gregory 1999, personal communication).

5. Conclusions

We have been concerned here with two quite distinct aspects of sea level rise in ocean GCMs: namely, the global trend in sea level rise over the decadal-to-century timescales and the spatial pattern of sea level rise variations about this global mean. Methods have been developed that enable us to characterize these two quantities in the output of fully coupled GCMs.

For the trend model, we have taken the density-layer levels from the thermal expansion ocean model of Church et al. (1991) and have analyzed the results of two tracer experiments in these layers in a global ocean GCM. The responses have been combined with thermal expansion coefficients calculated from a coupled ocean-atmosphere GCM to obtain estimates of the mixed-layer expansion coefficients and sea level rise Green's functions for the sea level response of the ocean to sea surface temperature forcing. One of these experiments includes the TRM parameterization of eddies, as described by McDougall and McIntosh (1996) and Gent and McWilliams (1990). The effect of this parameterization in ocean GCMs has been to quite impressively improve such fundamental ocean characteristics as the mixed-layer depth and the properties of deep water: the results from models with the TRM parameterization accord much better with reality than those without. In the case of the global trend in sea level, the inclusion of this TRM parameterization translates into a substantial decrease in future estimates of sea level rise (12%).

Despite the oceanic improvements resulting from the use of TRM, the ocean in both stand-alone and coupled modes still differs significantly from the observations [see Hirst et al. (2000) for a detailed discussion of the coupled model solution and England and Rahmstorf (1999) regarding the stand-alone ocean model]. There are several possible reasons for these differences, including the coarseness of the resolution and the lack of explicit parameterization for some oceanic processes (e.g., downslope flow). Our study also uses preexisting integrations spun up using surface restoring toward climatological $T-S$. This equilibration technique remains widely used because of uncertainties in direct heat and freshwater flux climatologies. Nevertheless, Large et al. (1997) found improvements in their model when bulk flux forcing was adopted. Clearly the Green's functions may be affected by these model-observation differences. Further, the coupled model uses flux corrections, which could bias climate change patterns, especially near the sea-ice margins. The testing of the Green's function method using improved models with higher

resolution and with reduced flux correction (or none), and an examination of the impact of spinup techniques on the resulting sea level calculations, are topics for future work.

The trend model of ocean heat uptake produces estimates of sea level rise that underestimate by roughly 10% the sea level rise signals seen in the TRM versions of CSIRO's fully coupled GCM. We have the aforementioned caveats associated with the various ocean models used in this study. However, this difference can also be attributed to the fact that we are making a comparison of sea level rise estimates made from an ocean running with today's climate with others made from transient fully coupled climate experiments in which the surface forcing is different.

Maps of the spatial pattern of sea level rise can be made from the output of coupled GCMs using a simple inverse method. It is shown that the solution obtained using this inverse method is more accurate than the solution obtained by using a simpler technique for finding the spatial map of pressure at a certain depth. Again, the inclusion of TRM physics in the ocean GCMs gives rise to striking differences in the global maps of sea level rise.

REFERENCES

- Anderssen, R. S., and F. R. deHoog, 1984: Finite difference methods for the numerical differentiation of non-exact data. *Computing*, **33**, 259–267.
- Bindoff, N. L., and T. J. McDougall, 1994: Diagnosing climate change and ocean ventilation using hydrographic data. *J. Phys. Oceanogr.*, **24**, 1137–1152.
- Böning, C. W., W. R. Holland, F. O. Bryan, G. Danabasoglu, and J. C. McWilliams, 1995: An overlooked problem in model simulations of the thermohaline circulation and heat transport in the Atlantic Ocean. *J. Climate*, **8**, 515–523.
- Bryan, K., 1969: A numerical method for the study of the circulation of the world ocean. *J. Comput. Phys.*, **3**, 347–376.
- , 1996: The steric component of sea-level rise associated with enhanced greenhouse warming: A model study. *Climate Dyn.*, **12**, 545–555.
- Butkovskiy, A. G., 1982: *Green's Functions and Transfer Functions Handbook*. Wiley and Sons, 236 pp.
- Church, J. A., J. S. Godfrey, D. R. Jackett, and T. J. McDougall, 1991: A model of sea-level rise caused by ocean thermal expansion. *J. Climate*, **4**, 438–456.
- Cox, M. D., 1984: A primitive equation, three-dimensional model of the ocean. GFDL Ocean Group Tech. Rep. 1, 143 pp. [Available from Princeton University, GFDL, Route 1, Forrestal Campus, Princeton, NJ 08542.]
- , 1987: Isopycnal diffusion in a z -coordinate ocean model. *Ocean Modelling* (unpublished manuscripts), **74**, 1–5.
- Cubasch, U., K. Hasselmann, H. Hock, E. Maier-Reimer, U. Mikolajewicz, B. D. Santer, and R. Sausen, 1992: Time dependent greenhouse warming computations with a coupled ocean-atmosphere model. *Climate Dyn.*, **8**, 55–69.
- , and Coauthors, 1994: Monte Carlo climate change forecasts with a global coupled ocean-atmosphere model. *Climate Dyn.*, **10**, 1–19.
- Danabasoglu, G., and J. C. McWilliams, 1995: Sensitivity of the global ocean circulation to parameterizations of mesoscale tracer transports. *J. Climate*, **8**, 2967–2987.

- , —, and P. R. Gent, 1994: The role of mesoscale tracer transports in the global ocean circulation. *Science*, **264**, 1123–1126.
- Duffy, P. B., P. Eltgroth, and A. J. Bourgeois, 1995: Improved representation of vertical profiles of temperature and bomb radiocarbon in the GFDL ocean general circulation model. *Geophys. Res. Lett.*, **22**, 1065–1068.
- England, M. H., 1993: Representing the global-scale water masses in ocean general circulation models. *J. Phys. Oceanogr.*, **23**, 1523–1552.
- , 1995: Using chlorofluorocarbons to assess ocean climate models. *Geophys. Res. Lett.*, **22**, 3051–3054.
- , and A. C. Hirst, 1997: Chlorofluorocarbon uptake in a World Ocean model. Part 2. Sensitivity to surface thermohaline forcing and subsurface mixing parameterizations. *J. Geophys. Res.*, **102**, 15 709–15 731.
- , and G. Holloway, 1998: Simulations of CFC content and water-mass age in the deep North Atlantic. *J. Geophys. Res.*, **103**, 15 885–15 902.
- , and S. Rahmstorf, 1999: Sensitivity of ventilation rates and radiocarbon uptake to subgrid-scale mixing in ocean models. *J. Phys. Oceanogr.*, **29**, 2802–2827.
- , V. C. Garçon, and J.-F. Minster, 1994: Chlorofluorocarbon uptake in a World Ocean model. Part 1. Sensitivity to the surface gas forcing. *J. Geophys. Res.*, **99**, 25 215–25 233.
- Gargett, A. E., 1984: Vertical eddy diffusivity in the ocean interior. *J. Mar. Res.*, **42**, 359–393.
- Gent, P. R., and J. C. McWilliams, 1990: Isopycnal mixing in ocean circulation models. *J. Phys. Oceanogr.*, **20**, 150–155.
- , J. Willebrand, T. J. McDougall, and J. C. McWilliams, 1995: Parameterizing eddy-induced tracer transports in ocean circulation models. *J. Phys. Oceanogr.*, **25**, 463–474.
- Gordon, H. B., and S. P. O'Farrell, 1997: Transient climate change in the CSIRO coupled model with dynamical sea ice. *Mon. Wea. Rev.*, **125**, 875–907.
- Greenberg, M. D., 1971: *Application of Green's Functions in Science and Engineering*. Prentice-Hall, 141 pp.
- Gregory, J. M., 1993: Sea level changes under increasing atmospheric CO₂ in a transient coupled ocean–atmosphere GCM experiment. *J. Climate*, **6**, 2247–2262.
- Hasselmann, K., R. Sausen, E. Maier-Reimer, and R. Voss, 1993: On the cold start problem in transient simulations with coupled atmosphere–ocean models. *Climate Dyn.*, **9**, 53–61.
- Hellerman, S., and M. Rosenstein, 1983: Normal monthly wind stress over the World Ocean with error estimates. *J. Phys. Oceanogr.*, **13**, 1093–1104.
- Hirst, A. C., 1999: The Southern Ocean response to global warming in the CSIRO coupled ocean–atmosphere model. *Environmental Modeling and Software: Special Issue on Global Climate Change*, R. J. Oglesby, Ed., Vol. 14, Elsevier, 227–241.
- , and W. Cai, 1994: Sensitivity of a World Ocean GCM to changes in subsurface mixing parameterization. *J. Phys. Oceanogr.*, **24**, 1256–1279.
- , and T. J. McDougall, 1996: Deep water properties and surface buoyancy flux as simulated by a z-coordinate model including eddy-induced advection. *J. Phys. Oceanogr.*, **26**, 1320–1343.
- , and —, 1998: Meridional overturning and diapycnal transport in a z-coordinate ocean model including eddy-induced advection. *J. Phys. Oceanogr.*, **28**, 1205–1223.
- , D. R. Jackett, and T. J. McDougall, 1996a: The meridional overturning cells of a world ocean model in neutral density coordinates. *J. Phys. Oceanogr.*, **26**, 775–791.
- , H. G. Gordon, and S. P. O'Farrell, 1996b: Global warming in a coupled climate model including oceanic eddy-induced advection. *Geophys. Res. Lett.*, **23**, 3361–3364.
- , —, and —, 2000: Comparison of a coupled ocean–atmosphere model with and without oceanic eddy-induced advection. Part I: Ocean spinup and control integrations. *J. Climate*, **13**, 139–163.
- IPCC, 1990: *Climate Change: The IPCC Scientific Assessment*. J. T. Houghton et al., Eds., Cambridge University Press, 364 pp.
- , 1992: *Climate Change 1992: The Supplementary Report to the IPCC Scientific Assessment*. J. T. Houghton et al., Eds., Cambridge University Press, 200 pp.
- , 1996: *Climate Change 1995: The Science of Climate Change*. J. T. Houghton et al., Eds., Cambridge University Press, 572 pp.
- Jackett, D. R., and T. J. McDougall, 1997: A neutral density variable for the world's oceans. *J. Phys. Oceanogr.*, **27**, 237–263.
- Kattenberg, A., and Coauthors, 1996: Climate models—Projections of future climate. *Climate Change 1995: The Science of Climate Change*. J. T. Houghton et al., Eds., Cambridge University Press, 285–357.
- Killworth, P. D., 1983: Deep convection in the World Ocean. *Rev. Geophys. Space Phys.*, **21**, 1–26.
- Large, W. G., G. Danabasoglu, S. C. Doney, and J. C. McWilliams, 1997: Sensitivity to surface forcing and boundary layer mixing in a global ocean model: Annual-mean climatology. *J. Phys. Oceanogr.*, **27**, 2418–2447.
- Levitus, S., 1982: *Climatological Atlas of the World Ocean*. National Oceanic and Atmospheric Administration, 173 pp. and 17 microfiche.
- Manabe, S., and R. J. Stouffer, 1994: Multiple-century response of a coupled ocean–atmosphere model to an increase of atmospheric carbon dioxide. *J. Climate*, **7**, 5–23.
- , —, M. J. Spelman, and K. Bryan, 1991: Transient responses of a coupled ocean–atmosphere model to gradual changes of atmospheric carbon dioxide. Part I: Annual mean response. *J. Climate*, **4**, 785–818.
- , M. J. Spelman, and R. J. Stouffer, 1992: Transient responses of a coupled ocean–atmosphere model to gradual changes of atmospheric carbon dioxide. Part II: Seasonal response. *J. Climate*, **5**, 105–126.
- McCartney, M. S., 1977: Subantarctic mode water. *A Voyage of Discovery: George Deacon 70th Anniversary Volume (Deep Sea Res. Suppl.)*, M. V. Angel, Ed., Pergamon, 103–119.
- McDougall, T. J., and J. A. Church, 1986: Pitfalls with the numerical representation of isopycnal and diapycnal mixing. *J. Phys. Oceanogr.*, **16**, 196–199.
- , and P. C. McIntosh, 1996: The temporal-residual-mean velocity. Part I: Derivation and the scalar conservation equations. *J. Phys. Oceanogr.*, **26**, 2653–2665.
- Mitchell, J. F. B., and T. C. Johns, 1997: On modification of global warming by sulfate aerosols. *J. Climate*, **10**, 245–267.
- Murphy, J. M., 1995: Transient response of the Hadley Centre coupled model to increasing carbon dioxide. Part III: Analysis of global-mean response using simple models. *J. Climate*, **8**, 496–514.
- O'Farrell, S. P., 1998: Sensitivity study of a dynamical sea ice model: The effect of the external stresses and land boundary conditions on ice thickness distribution. *J. Geophys. Res.*, **103**, 15 751–15 782.
- Olbers, D., V. Gouretzki, G. Seuß, and J. Schroeter, 1992: *The Hydrographic Atlas of the Southern Ocean*. Alfred-Wegener-Institute for Polar and Marine Research, 82 pp.
- Pacanowski, R. C., K. W. Dixon, and A. Rosati, 1991: The GFDL Modular Ocean Model users guide version 1.0. GFDL Ocean Group Tech. Rep. 2, 46 pp. [Available from Princeton University, GFDL, Route 1, Forrestal Campus, Princeton, NJ 08542.]
- Raper, S. C. B., and U. Cubasch, 1996: Emulation of the results from a coupled general circulation model using a simple climate model. *Geophys. Res. Lett.*, **23**, 1107–1110.
- , T. M. L. Wigley, and R. A. Warwick, 1996: Global sea-level rise: Past and future. *Rising Sea Level and Subsiding Coastal Areas*, J. D. Milliman and B. U. Huq, Eds., Kluwer Academic Publishers, 11–45.

- Redi, M. H., 1982: Oceanic isopycnal mixing by coordinate rotation. *J. Phys. Oceanogr.*, **12**, 1154–1158.
- Robitaille, D. Y., and A. J. Weaver, 1995: Validation of sub-grid scale mixing schemes using CFCs in a global ocean model. *Geophys. Res. Lett.*, **22**, 2917–2920.
- Shine, K. P., R. G. Derwent, D. J. Wuebbles, and J.-J. Morcrette, 1990: Radiative forcing of climate. *Climate Change: The IPCC Scientific Assessment*, J. T. Houghton et al., Eds., Cambridge University Press, 49–68.
- Stouffer, R. J., S. Manabe, and K. Bryan, 1989: Interhemispheric asymmetry in climate response to a gradual increase of atmospheric CO₂. *Nature*, **342**, 660–662.
- Veronis, G., 1975: The role of models in tracer studies. *Numerical Models of the Ocean Circulation*, National Academy of Sciences, 133–146.
- Wigley, T. M. L., and S. C. B. Raper, 1987: Thermal expansion of sea level associated with global warming. *Nature*, **330**, 127–131.
- , and —, 1992: Implications for climate and sea level of revised IPCC emissions scenarios. *Nature*, **357**, 293–300.
- , and —, 1993: Future changes in global mean temperature and sea level. *Climate and Sea Level: Observations, Projections and Implications*, R. A. Warwick et al., Eds., Cambridge University Press, 111–133.